Joint Emission–Based Patient and Hardware Attenuation Correction for non–TOF PET/MR Imaging

Thorsten Heußer, Christopher M. Rank, Yannick Berker, Martin T. Freitag, and Marc Kachelrieß

***Abstract*—Accurate PET quantification requires attenuation correction (AC) for photon attenuation within the patient and within hardware components located between patient and detector. AC is a major challenge in hybrid PET/MR imaging, since standard MR images do not provide direct information on both patient and hardware attenuation. Conventional MR–based AC (MRAC) employed in clinical routine does not properly consider bone attenuation and entirely neglects attenuation of flexible hardware components such as MR–safe headphones. Both effects result in severe activity underestimation, especially in the brain region, making accurate PET quantification difficult. We have recently proposed two modifications of the maximum–likelihood reconstruction of attenuation and activity (MLAA) algorithm for non time–of–flight (TOF) PET/MR, simultaneously reconstructing attenuation and activity distributions from the PET emission data. MR–MLAA aims at improving patient attenuation estimation by incorporating MR–derived prior expectations on the attenuation coefficients. The second algorithm, xMLAA, aims at estimating attenuation of flexible hardware components, without modifying the patient attenuation map. Both algorithms have been shown to significantly improve PET quantification compared to standard MRAC. In this work, MR–MLAA and xMLAA are combined to xMR–MLAA and applied to clinical PET/MR data of the head region. Compared to xMR–MLAA, conventional MRAC underestimates the average activity evaluated in the full brain by up to 15 %.**

***Index Terms*—Hybrid PET/MR Imaging, Attenuation Correction, MLAA**

I. Introduction

ACCURATE quantification in positron emission tomography (PET) requires correction of the acquired emission data for attenuation of the 511 keV annihilation photons within both the patient and the system hardware. This process, which is known as attenuation correction (AC), is a major challenge in hybrid PET/magnetic resonance (MR) imaging, since a direct conversion of the MR information into PET attenuation coefficients is not possible [1]. The standard approach for MR–based AC (MRAC) currently employed in clinical routine is to use dedicated MR information to segment three or four tissue classes, which are then assigned pre–defined attenuation coefficients [2, 3]. Bone attenuation is typically treated as soft tissue, resulting in an underestimation of the reconstructed PET activity distribution, with regional underestimation values as high as 20 % [4]. Recent publications have demonstrated significant improvements on PET quantification by incorporating accurate bone attenuation information employing altas–based methods [5, 6] or using dedicated MR sequences, e.g., ultrashort–echo–time (UTE) sequences [7].

AC of stationary hardware components such as patient table and MR head/neck coils is straightforward, using pre–acquired CT–based attenuation templates converted to 511 keV [8]. For flexible components, such as MR torso surface coils or MR–safe headphones, AC is more challenging, as the corresponding hardware attenuation maps need to be scan–specific. Registration–based approaches have been proposed [9, 10], but are currently not used in clinical routine. Neglecting attenuation of flexible hardware components during AC has been shown to result in regional activity underestimation of up to 16 % in case of MR–safe headphones [11, 12].

We have recently proposed two modifications of the maximum–likelihood reconstruction of attenuation and activity (MLAA) algorithm [13] dedicated for non time–of–flight (TOF) PET/MR imaging [14, 15]. Both algorithms simultaneously reconstruct attenuation and activity distributions from the PET emission data. MR–MLAA aims at improving patient attenuation by incorporating voxel–specific MR–derived prior expectations on the attenuation coefficients [14]. The second algorithm, called external MLAA (xMLAA), estimates the attenuation of flexible hardware components such as the MR–safe headphones without modifying the patient attenuation map [15].

In this work, we propose a combination of MR–MLAA and xMLAA for improved attenuation estimation and thus PET quantification in hybrid PET/MR imaging. The joint algorithm, referred to as xMR–MLAA, does not require time–of–fight (TOF) information. Moreover, to keep the clinical workflow as simple as possible, non–conventional MR sequences such as UTE are not required. We present xMR–MLAA results for patient data acquired with a clinical hybrid non–TOF PET/MR device (Biograph mMR, Siemens Healthineers, Erlangen, Germany) and compare with standard MRAC and CT–based AC (CTAC). The evaluated patient data correspond to the head region and xMR–MLAA is applied to estimate both patient and headphone attenuation.

Thorsten Heußer, Dr. Christopher M. Rank, and Prof. Dr. Marc Kachelrieß: Medical Physics in Radiology, German Cancer Research Center (DKFZ), 69120 Heidelberg, Germany.

Dr. Yannick Berker: Physics of Molecular Imaging Systems, RWTH Aachen University, 52074 Aachen, Germany and Department of Radiology, University of Pennsylvania, Philadelphia, PA 19104, USA.

Dr. Martin T. Freitag: Department of Radiology, German Cancer Research Center (DKFZ), 69120 Heidelberg, Germany.

Corresponding author: thorsten.heusser@dkfz.de.

DOI: 10.12059/Fully3D.2017-11-3103001

II. Materials and Methods

A. Objective Function

The proposed xMR–MLAA algorithm aims at simulteneously reconstructing the activity image $\boldsymbol{\lambda} = (\lambda_1, \cdots, \lambda_I)^{\mathrm{T}}$ and the attenuation image $\boldsymbol{\mu} = (\mu_1, \cdots, \mu_I)^{\mathrm{T}}$ from the PET emission data $\boldsymbol{p} = (p_1, \cdots, p_J)^{\mathrm{T}}$, where I gives the number of image voxels and J specifies the number of line–of–responses (LORs). The algorithm is iterative, seeking to optimize the objective function

$$Q(\boldsymbol{\lambda}, \boldsymbol{\mu}) = L(\boldsymbol{\lambda}, \boldsymbol{\mu}) + L_{\mathrm{S}}(\boldsymbol{\mu}) + L_{\mathrm{I}}(\boldsymbol{\mu}). \tag{1}$$

$L(\boldsymbol{\lambda}, \boldsymbol{\mu})$ is the log–likelihood function, which is given as

$$L(\boldsymbol{\lambda}, \boldsymbol{\mu}) = \sum_j (p_j \ln \hat{p}_j - \hat{p}_j), \tag{2}$$

where

$$\hat{p}_j = \frac{1}{a_j n_j} \sum_i M_{ij} \lambda_i + \frac{s_j}{n_j} + r_j \tag{3}$$

are the expected number of coincidences along LOR j. In equation (3), M_{ij} specifies the elements of the system matrix, and n_j, s_j, and r_j represent normalization, scatter, and randoms contribution to LOR j, respectively. The attenuation correction factor (ACF) for LOR j is given by

$$a_j = \exp\big(\sum_i l_{ij} \mu_i\big), \tag{4}$$

where l_{ij} denotes the intersection length of voxel i with LOR j.

B. Prior Information

The objective function (1) includes two prior terms. The smoothing prior $L_{\mathrm{S}}(\boldsymbol{\mu})$ penalizes differences in the attenuation coefficients of neighboring voxels. The intensity prior

$$L_{\mathrm{I}}(\boldsymbol{\mu}) = \omega_{\mathrm{x}}(\boldsymbol{r}) \beta_{\mathrm{x}} L_{\mathrm{x}}(\boldsymbol{\mu}) + (1 - \omega_{\mathrm{x}}(\boldsymbol{r})) L_{\mathrm{MR}}(\boldsymbol{\mu}), \tag{5}$$

is a linear combination of the xMLAA intensity prior $L_{\mathrm{x}}(\boldsymbol{\mu})$ and the MR–MLAA intensity prior $L_{\mathrm{MR}}(\boldsymbol{\mu})$, which have been proposed in our previous work [14, 15]. In equation (5), the weighting parameter $\omega_{\mathrm{x}}(\boldsymbol{r})$ represents the so–called hardware mask, which is set to zero within the MR–derived patient support and set to one within the region where the hardware components are assumed to be located. In case of the headphones, this region corresponds to the interior of the MR head coil. The xMLAA intensity prior $L_{\mathrm{x}}(\boldsymbol{\mu})$ is realized as the logarithm of a bi–modal, Gaussian–like probability distribution, defining expectations on mean and distribution of air and hardware attenuation coefficients, as explained in more detail in our previous work [15].

The MR–MLAA intensity prior is defined as

$$L_{\mathrm{MR}}(\boldsymbol{\mu}) = \omega_{\mathrm{MR}}(\boldsymbol{r}) \beta_{\mathrm{ST}} L_{\mathrm{ST}}(\boldsymbol{\mu}) + (1 - \omega_{\mathrm{MR}}(\boldsymbol{r})) \beta_{\mathrm{AB}} L_{\mathrm{AB}}(\boldsymbol{\mu}). \tag{6}$$

Here, $\omega_{\mathrm{MR}}(\boldsymbol{r})$ defines the so–called patient attenuation mask, which is derived from available MR information. In this work, conventional diagnostic T1–weighted MR images are employed for mask generation. The patient attenuation mask is comprised of two segments: one segment contains all voxels assumed to represent either air or bone (AB). The other segment contains voxels which are assumed to correspond to soft tissue (ST). The corresponding prior terms L_{AB} and L_{ST} incorporate pre–defined expectations on the mean values and the distribution of the attenuation coefficients corresponding to air, bone, and soft tissue, respectively. More details are found in our previous work [14]. The patient attenuation mask is set to $\omega = 0$ for the AB segment and to $\omega = 1$ for the ST segment. Intermediate values are obtained by Gaussian smoothing of the mask.

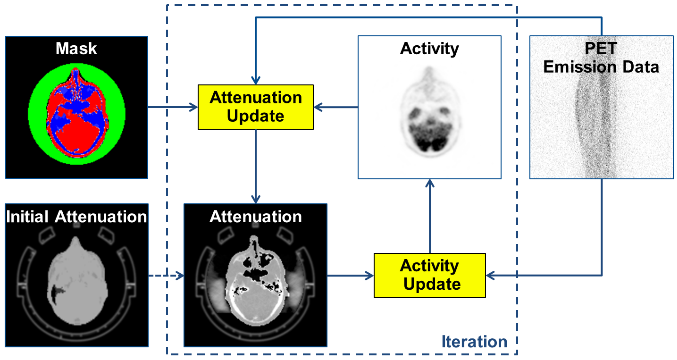

Fig. 1. General flowchart of the proposed xMR–MLAA algorithm. The approach is iterative, updating activity and attenuation in an alternating manner. The MR–derived mask defines the regions where the hardware components are assumed to be located (green), and where attenuation coefficients corresponding to soft tissue (red) and air or bone (blue) are expected.

In equation (1), both prior terms are functions of the attenuation distribution $\boldsymbol{\mu}$ only and do not depend on the activity distribution $\boldsymbol{\lambda}$. As a consequence, the priors will only affect the attenuation update while the activity update is not affected. In equations (5) and (6), the parameters β_{x}, β_{ST}, and β_{AB}, can be used to vary the strength of the individual components of the intensity prior with respect to the log–likelihood term given by (2).

C. xMR–MLAA Workflow

Solving for the activity distribution $\boldsymbol{\lambda}$ and the attenuation distribution $\boldsymbol{\mu}$ is done by iterative optimization of the objective function (1), alternately updating $\boldsymbol{\lambda}$ while keeping $\boldsymbol{\mu}$ constant and vice versa. A general flowchart of the proposed xMR–MLAA algorithm is given in figure 1. The activity update is performed employing ordinary–Poisson ordered subset expectation maximization (OP–OSEM) [16]. For the attenuation update, a gradient–ascent method for transmission tomography [17] is employed. For more details on the update equations, please refer to our previous work [14].

In this work, hardware and patient attenuation estimation are performed in an interleaved manner. First, an estimate of the headphone attenuation is obtained (2 iterations, 21 subsets), employing the attenuation update only within the hardware mask, i.e., patient attenuation map and stationary hardware components are not modified. The estimated headphone attenuation map is added to the vendor–provided hardware attenuation map including patient table and MR head coil. Then, the patient attenuation map is estimated, applying the attenuation update only within the volume defined by the patient support (3 iterations, 21 subsets). The estimated attenuation

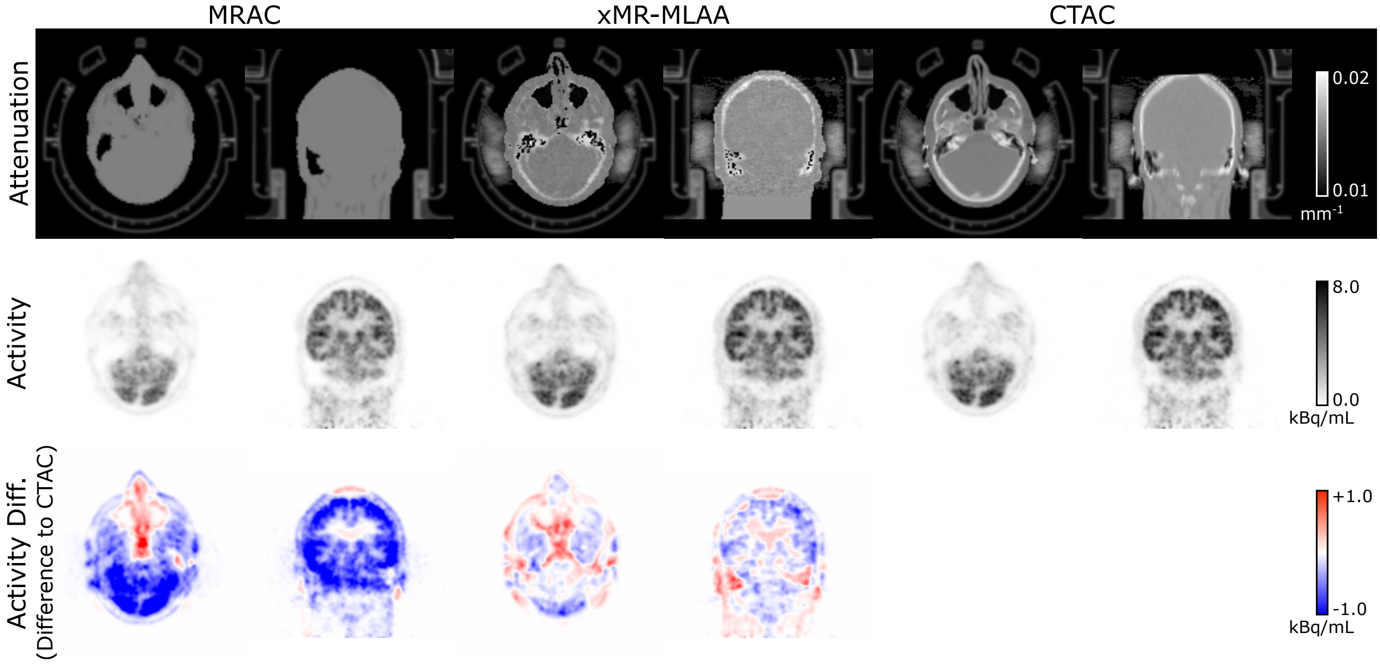

Fig. 2. Transversal and coronal views of MRAC, MR–MLAA, and CTAC attenuation maps and corresponding activity distributions. The last row gives the activity difference compared to CTAC.

distribution is refined, performing one additional iteration (21 subsets) for each headphone and patient attenuation.

D. *Experiments*

We evaluate the proposed xMR–MLAA algorithm for clinical PET/MR data acquired with a Siemens Biograph mMR. The measured PET data do not contain TOF information. For derivation of the patient support and the patient attenuation mask, conventional diagnostic T1–weighted MR images are used. The proposed approach is evaluated for three FDG and one FET patient data set of the head region. Each patient was wearing vendor–provided MR–safe pneumatic headphones during data acquisition.

III. Results

Figure 2 shows the xMR–MLAA results for one FDG patient. Standard MRAC results in activity underestimation in the brain, caused both by neglecting headphone attenuation and by treating bone as soft tissue during AC. Across three FDG patients included in this study, average brain activity underestimation was $14.8\,\%$ compared to CTAC. Using MR–MLAA, bone attenuation information can be accurately recovered while preserving air cavities like the nasal sinuses and the inner ears. The estimated headphones can clearly be identified. As seen in figure 2, PET quantification is significantly improved when using xMR–MLAA. Average brain activity underestimation with MR–MLAA was $2.8\,\%$ compared to CTAC across three FDG patients. Note, since no co–registered CT–based template of the headphones was available, the headphone attenuation estimate obtained by xMR–MLAA was added to the CT–based patient attenuation map. Thus, the differences between xMR–MLAA and CTAC are only due to different patient attenuation maps.

The impact of xMR–MLAA–based headphone attenuation on PET quantification is demonstrated in figure 3. Neglecting headphones during AC results in activity underestimation, especially in the region embraced by the earpads of the headphones. As stated previously, a quantitative evaluation was difficult since no co–registered CT–based headphone attenuation map was available in case of clinical data. We therefore compare the results obtained for three FDG and one FET patient with a phantom study, where the accuracy of xMR–MLAA–based headphone attenuation estimation has been presented in our previous work [15]. For the region

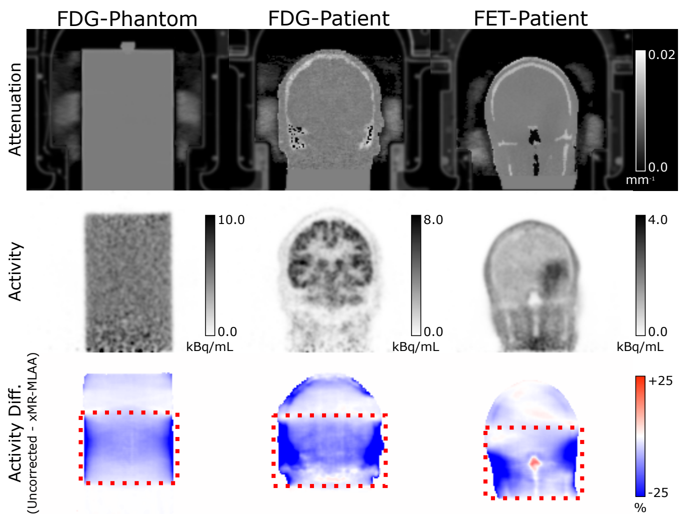

Fig. 3. Impact of headphone attenuation estimated with xMR–MLAA for a phantom study and for clinical FDG and FET data. The last row gives the relative difference of the activity images reconstructed without headphones (uncorrected, not shown) and with headphones (middle row).

embraced by the earpads, illustrated by the red boxes in figure 3, neglecting the headphones during AC resulted in average activity underestimation of $7.9\,\%$ in case of the phantom study, of $9.2\,\%$ across the three FDG data sets, and of $8.4\,\%$ in case of the FET patient. This shows that the effect of the headphone attenuation estimated with xMR–MLAA is comparable for phantom and patient data.

IV. Discussion and Conclusion

The combination of MR–MLAA [14] and xMLAA [15] to the novel xMR–MLAA algorithm can be employed to obtained accurate estimates of both patient and hardware attenuation maps. Average activity underestimation in the brain is found to be as high as $15\,\%$ for standard MRAC, which neglects hardware attenuation and does not properly account for bone attenuation. Our preliminary results indicate that PET quantification errors in the brain can be reduced to below $3\,\%$ employing the proposed xMR–MLAA algorithm. However, for a thorough comparison, co–registered CT–based attenuation templates of the hardware components are required.

Acknowledgment

This work was supported by the Helmholtz International Graduate School for Cancer Research, Heidelberg, Germany. Parts of the reconstruction software was provided by RayConStruct® GmbH, Nürnberg, Germany.

References

[1] A. Mehranian, H. Arabi, and H. Zaidi, "Vision 20/20: Magnetic resonance imaging-guided attenuation correction in PET/MRI: Challenges, solutions, and opportunities," *Med. Phys.*, vol. 43, no. 3, pp. 1130–55, 2016.

[2] A. Martinez-Möller, M. Souvatzoglou, G. Delso, R. A. Bundschuh, C. Chefd'hotel, S. I. Ziegler, N. Navab, M. Schwaiger, and S. G. Nekolla, "Tissue classification as a potential approach for attenuation correction in whole-body PET/MRI: evaluation with PET/CT data." *J. Nucl. Med.*, vol. 50, no. 4, pp. 520–6, 2009.

[3] T. Beyer, M. L. Lassen, R. Boellaard, G. Delso, M. Yaqub, B. Sattler, and H. H. Quick, "Investigating the state–of–the–art in whole–body MR-based attenuation correction: an intra–individual, inter–system, inventory study on three clinical PET/MR systems," *MAGMA*, vol. 29, no. 1, pp. 75–87, 2016.

[4] M. Aznar, R. Sersar, J. Saabye, C. N. Ladefoged, F. L. Andersen, J. Rasmussen, J. Löfgren, and T. Beyer, "Whole–body PET/MRI: The effect of bone attenuation during MR–based attenuation correction in oncology imaging," *Eur. J. Radiol.*, vol. 83, no. 7, pp. 1177–83, 2014.

[5] N. Burgos, M. J. Cardoso, K. Thielemans, M. Modat, S. Pedemonte, J. Dickson, A. Barnes, R. Ahmed, C. J. Mahoney, J. M. Schott, J. S. Duncan, D. Atkinson, S. R. Arridge, B. F. Hutton, and S. Ourselin, "Attenuation Correction Synthesis for Hybrid PET–MR Scanners: Application to Brain Studies," *IEEE Trans. Med. Imaging*, vol. 33, no. 12, pp. 2332–41, 2014.

[6] D. H. Paulus, H. H. Quick, C. Geppert, M. Fenchel, Y. Zhan, G. Hermosillo, D. Faul, F. Boada, K. P. Friedman, and T. Koesters, "Whole–Body PET/MR Imaging: Quantitative Evaluation of a Novel Model–Based MR Attenuation Correction Method Including Bone," *J. Nucl. Med.*, vol. 56, no. 7, pp. 1061–6, 2015.

[7] C. N. Ladefoged, D. Benoit, I. Law, S. Holm, A. Kjær, L. Højgaard, A. E. Hansen, and F. L. Andersen, "Region specific optimization of continuous linear attenuation coefficients based on UTE (RESOLUTE): application to PET/MR brain imaging," *Phys. Med. Biol.*, vol. 60, no. 20, pp. 8047–65, 2015.

[8] B. Zhang, D. Pal, Z. Hu, N. Ojha, T. Guo, G. Muswick, C. H. Tung, and J. Kaste, "Attenuation correction for MR table and coils for a sequential PET/MR system," in *IEEE Nucl. Sci. Symp. Conf. Rec.*, 2009, pp. 3303–6.

[9] G. Delso, A. Martinez-Möller, R. A. Bundschuh, R. Ladebeck, Y. Candidus, D. Faul, and S. I. Ziegler, "Evaluation of the attenuation properties of MR equipment for its use in a whole–body PET/MR scanner," *Phys. Med. Biol.*, vol. 55, no. 15, pp. 4361–74, 2010.

[10] D. H. Paulus, H. Braun, B. Aklan, and H. H. Quick, "Simultaneous PET/MR imaging: MR–based attenuation correction of local radiofrequency surface coils." *Med. Phys.*, vol. 39, no. 7, pp. 4306–15, 2012.

[11] A. Ferguson, J. McConathy, Y. Su, D. Hewing, and R. Laforest, "Attenuation Effects of MR Headphones During Brain PET/MR Studies," *J. Nucl. Med. Technol.*, vol. 42, no. 2, pp. 93–100, 2014.

[12] F. Büther, A. Vrachimis, A. Becker, and L. Stegger, "Impact of MR–safe headphones on PET attenuation in combined PET/MRI scans," *EJNMMI Research*, vol. 6, p. 20, 2016.

[13] J. Nuyts, P. Dupont, S. Stroobants, R. Benninck, L. Mortelmans, and P. Suetens, "Simultaneous maximum a posteriori reconstruction of attenuation and activity distributions from emission sinograms." *IEEE Trans. Med. Imaging*, vol. 18, no. 5, pp. 393–403, 1999.

[14] T. Heußer, C. M. Rank, M. T. Freitag, A. Dimitrakopoulou-Strauss, H.-P. Schlemmer, T. Beyer, and M. Kachelrieß, "MR–Consistent Simultaneous Reconstruction of Attenuation and Activity for Non–TOF PET/MR," *IEEE. Trans. Nucl. Sci.*, vol. 63, no. 5, pp. 2443–51, 2016.

[15] T. Heußer, C. M. Rank, M. T. Freitag, and M. Kachelrieß, "MLAA–Based Headphone Attenuation Estimation in Hybrid PET/MR Imaging," in *IEEE Nucl. Sci. Symp. Conf. Rec.*, 2016, pp. M10B–1.

[16] C. Comtat, F. Bataille, C. Michel, J. P. Jones, M. Sibomana, L. Janeiro, and R. Trébossen, "OSEM–3D Reconstruction Strategies for the ECAT HRRT," in *IEEE Nucl. Sci. Symp. Conf. Rec.*, 2004, pp. 3492–6.

[17] J. Nuyts, B. De Man, P. Dupont, M. Defrise, P. Suetens, and L. Mortelmans, "Iterative reconstruction for helical CT: a simulation study," *Phys. Med. Biol.*, vol. 43, no. 4, pp. 729–37, 1998.